frontiers in Chemistry

ORIGINAL RESEARCH
published: 18 March 2020
doi: 10.3389/fchem.2020.00129

Green and Facile Synthesis of Metal-Organic Framework Cu-BTC-Supported Sn (II)-Substituted Keggin Heteropoly Composites as an Esterification Nanocatalyst for Biodiesel Production

Qiuyun Zhang[1,2]*, *Dan Ling*[1], *Dandan Lei*[1], *Jialu Wang*[3]*, *Xiaofang Liu*[4], *Yutao Zhang*[2,3] *and Peihua Ma*[5]*

[1] School of Chemistry and Chemical Engineering, Anshun University, Anshun, China, [2] Engineering Technology Center of Control and Remediation of Soil Contamination of Provincial Science & Technology Bureau, Anshun University, Anshun, China, [3] School of Resource and Environmental Engineering, Anshun University, Anshun, China, [4] Food and Pharmaceutical Engineering Institute, Guiyang University, Guiyang, China, [5] School of Chemistry and Chemical Engineering, Guizhou University, Guiyang, China

OPEN ACCESS

Edited by:
Yaqiong Su,
Eindhoven University of Technology, Netherlands

Reviewed by:
Yeh-Yung Lin,
Dalian University of Technology, China
Ya-Long Ding,
Huanghuai University, China

***Correspondence:**
Qiuyun Zhang
qyzhang.asu@gmail.com
Jialu Wang
lu226@163.com
Peihua Ma
phma@gzu.edu.cn

Specialty section:
This article was submitted to Green and Sustainable Chemistry, a section of the journal Frontiers in Chemistry

Received: 08 January 2020
Accepted: 12 February 2020
Published: 18 March 2020

Citation:
Zhang Q, Ling D, Lei D, Wang J, Liu X, Zhang Y and Ma P (2020) Green and Facile Synthesis of Metal-Organic Framework Cu-BTC-Supported Sn (II)-Substituted Keggin Heteropoly Composites as an Esterification Nanocatalyst for Biodiesel Production. Front. Chem. 8:129. doi: 10.3389/fchem.2020.00129

In the present study, metal-organic framework Cu-BTC-supported Sn (II)-substituted Keggin heteropoly nanocomposite ($Sn_{1.5}PW$/Cu-BTC) was successfully prepared by a simple impregnation method and applied as a novel nanocatalyst for producing biodiesel from oleic acid (OA) through esterification. The nanocatalyst was characterized by Fourier transform infrared spectrometry (FTIR), wide-angle X-ray diffraction (XRD), scanning electron microscopy (SEM), transmission electron microscopy (TEM), nitrogen adsorption-desorption, thermogravimetrics (TG), and NH_3-temperature-programmed desorption (NH_3-TPD). Accordingly, the synthesized nanocatalyst with a $Sn_{1.5}PW$/Cu-BTC weight ratio of 1 exhibited a relatively large specific surface area, appropriate pore size, and high acidity. Moreover, an OA conversion of 87.7% was achieved under optimum reaction conditions. The nanocatalyst was reused seven times, and the OA conversion remained at more than 80% after three uses. Kinetic study showed that the esterification reaction followed first-order kinetics, and the activation energy (E_a) was calculated to be 38.3 kJ/mol.

Keywords: heteropolys, Cu-BTC, nanocomposites, esterification, biodiesel

INTRODUCTION

Nowadays, fossil fuel resource demand is expanding progressively due to industrial growth and constant population rise. Meanwhile, the utilization of fossil fuels along with environmental pollution and global warming has led to the consideration of alternative energy sources like biofuels (Bhanja and Bhaumik, 2016; Long et al., 2019; Negm et al., 2019; Xu et al., 2019; Li et al., 2020). Among the various biofuels, biodiesel is considered to be the most promising renewable

fuel, possibly due to its biodegradable, non-toxic, and environmentally friendly features (Al-Saadi et al., 2018; Li H. et al., 2019). Further, the typical way of producing biodiesel is the catalytic esterification of free fatty acids or transesterification of triglyceride with an alcohol in the presence of a homogeneous/heterogeneous catalyst (Mahmoud, 2019). A homogeneous acid catalyst, such as HCl, H_2SO_4, or H_3PO_4, can catalyze esterification with high activity; however, the major drawbacks of homogeneous acid catalysts are the generation of a huge amount of chemical wastewater and the high cost for catalyst separation and non-reusability (Zhang et al., 2019a). Therefore, heterogeneous solid catalysts have been widely applied to catalyze the esterification reaction for biodiesel synthesis.

One option is to use hetropolyacids as strong Brønsted acid catalysts for catalytic esterification and transesterification reactions to produce biodiesel with high conversions (Talebian-Kiakalaieh et al., 2013; Sun et al., 2015; Xie and Wan, 2019a). Unfortunately, hetropolyacids have certain disadvantages, such as good solubility in polar media and a low surface area (Parida and Mallick, 2007; Ekinci and Oktar, 2019). Therefore, supporting hetropolyacids on porous supports is an interesting approach to produce heterogeneous catalysts, since it can provide high surface area and insolubility in the polar solvent.

Various types of supported hetropolyacid catalysts have been utilized. Montmorillonite K10 (Nandiwale and Bokade, 2014), Nb_2O_5 (da Conceiçao et al., 2017), and carbon (Ghubayra et al., 2019) can be used as supports, but they were more or less subject to the disadvantages of weak interaction between object and host, low stability, high-cost synthesis, etc. By contrast, metal-organic frameworks (MOFs) provide excellent support, having the features of stability, adjustable tunnels, ultra-high specific surface area, and high catalytic efficiency (Kang et al., 2019; Li D. D. et al., 2019). Examples are PTA@MIL-53 (Fe) (Nikseresht et al., 2017), AILs/HPW/UiO-66-2COOH (Xie and Wan, 2019b), and $ZnFe_2O_4$/MIL-100(Fe) (Hu et al., 2019). Meanwhile, our previous studies showed the esterification of oleic acid or lauric acid with methanol over silicotungstic acid and nickel salts of Keggin-type heteropolyacids encapsulated into metal-organic framework (UiO-66) hybrid nanocatalysts that had excellent activity and reusability (Zhang et al., 2019b, 2020).

To date, there have been no reports on carrying out esterification reaction for biodiesel production using metal-organic framework Cu-BTC-supported Sn (II)-substituted Keggin heteropolyacids as nanocatalysts. Thus, in this work, we successfully synthesized a series of nanocatalysts consisting of Sn (II)-substituted 12-tungstophosphoric acid on a Cu-BTC matrix ($Sn_{1.5}$PW/Cu-BTC-x) at different ratios and used those nanocatalysts for producing biodiesel from OA with methanol. The characterization of synthesized nanocomposites was done using FTIR, XRD, SEM, TEM, nitrogen adsorption-desorption, TG, and NH_3-TPD. Further, the effect of different reaction parameters such as the molar ratio of methanol to OA, amount of catalyst, and reaction time and temperature were investigated to optimize the esterification conditions. Kinetic studies of the OA esterification reaction over the $Sn_{1.5}$PW/Cu-BTC nanocatalyst were studied. Finally, the reusability of those composites was also studied for seven successive runs.

EXPERIMENTAL SECTION

Materials and Synthesis

All chemicals were obtained from commercial sources and used without further purification. Copper (II) acetate monohydrate ($Cu(CO_2CH_3)_2{\cdot}H_2O$, AR), 1,3,5-benzenetricarboxylic acid (H_3-BTC) (AR), tin chloride dehydrate ($SnCl_2{\cdot}2H_2O$, AR), and 12-tungstophosphoric acid ($H_3PW_{12}O_{40}$, HPW, AR) were purchased from Shanghai Aladdin Industrial Inc. Oleic acid (OA, AR), N,N-dimethylformamide (DMF, AR), acetic acid (AR), absolute ethanol (AR), and anhydrous methanol (AR) were purchased from Sinopharm Chemical Reagent Co., Ltd.

Firstly, $Sn_{1.5}PW_{12}O_{40}$ ($Sn_{1.5}$PW) salts were prepared by stirring an aqueous solution containing the HPW and $SnCl_2$ at room temperature for 3 h; then, the obtained mixture was dried overnight at 120°C, according to our previous reports (Zhang et al., 2019a). Second, Cu-BTC was prepared from 0.06 g of copper (II) acetate monohydrate and 0.6 g of acetic acid dissolved in 6 mL distilled water, and 0.16 g of H_3-BTC dissolved in 6 mL of DMF was added dropwise from above the mixture solution. The resulting solution continued to be stirred for 3 h at room temperature. Then, the precipitate was collected by centrifugation and washed with 50 mL of hot ethanol two times and hot water once, and the blue powder was dried at 120°C for 12 h, according to the literature (Na et al., 2012). Finally, Cu-BTC-supported Sn (II)-substitute phosphotungstic acid catalysts were prepared by an impregnation method. $Sn_{1.5}$PW (0.25, 0.50, and 0.75 g) and the framework of Cu-BTC (0.50 g) at certain weight ratios were mixed in water. The obtained mixture was treated by ultrasonication for 10 min and was stirred continuously for 8 h at room temperature, followed by centrifugation and washing with distilled water three times. The resulting material was dried overnight in an oven (120°C). The synthesized $Sn_{1.5}$PW/Cu-BTC-x hybrids with different $Sn_{1.5}$PW to Cu-BTC weight ratios of 0.5, 1, and 1.5 were identified as $Sn_{1.5}$PW/Cu-BTC-0.5, $Sn_{1.5}$PW/Cu-BTC-1, and $Sn_{1.5}$PW/Cu-BTC-1.5, respectively.

Instrumentation

Fourier-transformed infrared spectroscopy (FTIR) spectra of the synthesized catalysts were obtained for powdered samples on KBr pellets using a PerkinElmer Spectrum 100 in the range of 400–4,000 cm^{-1}. Wide-angle X-ray diffraction (XRD) patterns were recorded on a D8 ADVANCE (Germany) using CuKI (1.5406 Å) radiation to get insight into the composition of the catalysts. The morphology of the catalysts was obtained on a scanning electron microscope (SEM) at 2.0 kV (Hitachi S4800) and a transmission electron microscope (TEM) at 200 kV (FEI Tecnai G2 20). The BET surface area and pore size were determined based on nitrogen adsorption-desorption isotherms with a Quantachrome instrument (Quantachrome Instruments, Boynton Beach, USA). Thermogravimetric (TG) analysis was carried out in a NETZSCH/STA 409 PC Luxx simultaneous thermal analyzer; the samples were heated up from room temperature to 600°C at a heating rate of 5°C/min. The acidic properties of the $Sn_{1.5}$PW/Cu-BTC-1

hybrid catalysts were characterized by temperature-programmed desorption (NH_3-TPD) (Micromeritics AutoChem II 2920).

Catalytic Evaluation

Using a typical approach, the esterification of OA and methanol was performed in a 50-ml stainless-steel high-pressure autoclave reactor, and an appropriate amount of catalyst was charged into the autoclave reactor. Then, the reactor was preheated in an oil bath with a magnetic stirrer at an appropriate temperature for a specific time. After completion of the reaction period, all catalysts were recovered by centrifugation at 8,000 rpm for 5–7 min and washed by anhydrous methanol. In order to calculate the OA conversion, the reactants were purified in a rotary evaporator to remove water and residual methanol. The conversion of methyl oleate was estimated by measuring the acid value of feedstock and product, and the acid value was determined according to the method described in the ISO 660-2009 standard (Animal and vegetable fats and oils—determination of acid value and acidity).

RESULTS AND DISCUSSION

Catalyst Characterization

The $Sn_{1.5}PW$, Cu-BTC, and $Sn_{1.5}PW$/Cu-BTC-x hybrids were firstly characterized by wide-angle XRD (**Figure 1**). For the $Sn_{1.5}PW$ sample, the peaks at 10.5°, 14.8°, 18.2°, 20.8°, 23.3°, 25.7°, 29.7°, 35.4°, and 38.0° can be related to the Keggin unit of HPW (Pasha et al., 2019), indicating the intact Keggin ion in the Sn-exchanged HPW catalysts. According to the literature (Yang et al., 2015), the wide-angle XRD spectrum of the synthesized Cu-BTC was in perfect agreement with the spectrum of simulated Cu-BTC. After supporting Sn (II)-substituted Keggin HPW, all $Sn_{1.5}PW$/Cu-BTC-x hybrids showed a decrease in the peak intensities of the Cu-BTC characteristic phase, and the XRD spectrum of $Sn_{1.5}PW$ could not be distinguished from the XRD spectra of $Sn_{1.5}PW$/Cu-BTC hybrids, suggesting that the $Sn_{1.5}PW$ salts were relatively uniformly distributed on the surface of Cu-BTC cages. Interestingly, the peak intensities of $Sn_{1.5}PW$/Cu-BTC-1 were much stronger than those of $Sn_{1.5}PW$/Cu-BTC-0.5 and $Sn_{1.5}PW$/Cu-BTC-1.5, which is probably due to the existence of interaction between the uniformly dispersed $Sn_{1.5}PW$ molecules and Cu-BTC matrix. These results showed that $Sn_{1.5}PW$ molecules were loaded on the surface of Cu-BTC nanocages through strong interaction.

The FTIR spectra of the HPW and $Sn_{1.5}PW$ samples were given in **Figure S1**. The FTIR spectra of HPW and Sn (II)-substituted HPW salts presented four characteristic peaks at 1,080, 982, 889, and 801 cm^{-1}, which was correlated with the Keggin unit of HPW, in agreement with the literature (Zhang et al., 2016). Moreover, as can be seen in **Figure 2**, the FTIR spectra of all $Sn_{1.5}PW$/Cu-BTC-x hybrids showed the peaks corresponding to Cu-BTC, the coordinated acac ligand showed peaks at 1,450 and 1,373 cm^{-1}, and some characteristic peaks at 1,645 and 1,586 cm^{-1} were shifted to 1,621 and 1,571 cm^{-1}, respectively, indicating strong interaction between $Sn_{1.5}PW$ and Cu-BTC nanoparticles. Surprisingly, the various $Sn_{1.5}PW$ concentrations for $Sn_{1.5}PW$/Cu-BTC showed four peaks at 1,080, 982, 889, and 801 cm^{-1}, respectively, further indicating that $Sn_{1.5}PW$ molecules were embedded around the surface of the Cu-BTC matrix. This also probably confirmed its stability and that it would suffer less leaching during the esterification reaction.

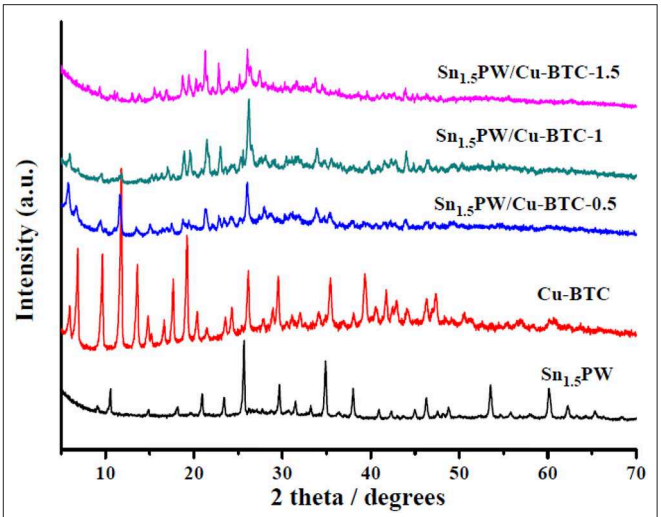

FIGURE 1 | Wide-angle XRD patterns of the $Sn_{1.5}PW$, Cu-BTC, and $Sn_{1.5}PW$/Cu-BTC-x hybrids.

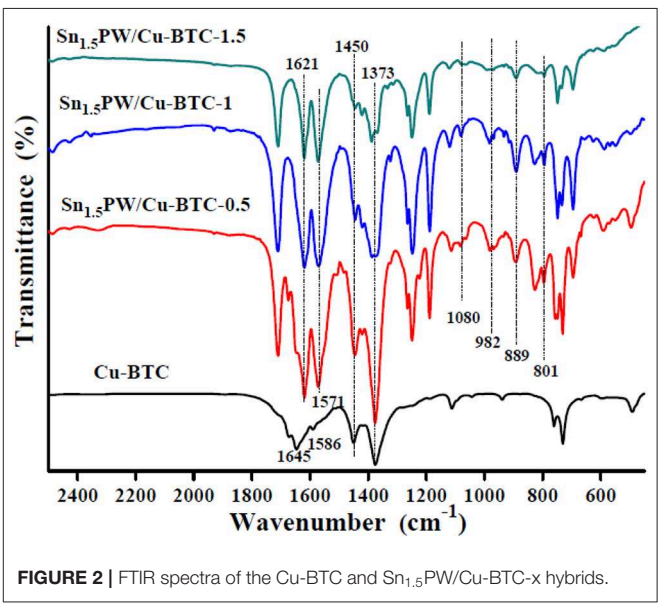

FIGURE 2 | FTIR spectra of the Cu-BTC and $Sn_{1.5}PW$/Cu-BTC-x hybrids.

Figure 3 shows the SEM images of the pure HPW, $Sn_{1.5}PW$, Cu-BTC, and $Sn_{1.5}PW$/Cu-BTC-x hybrids. The image of the pure HPW shows a large-blocked aggregate morphology. After Sn had been doped with HPW, the $Sn_{1.5}PW$ sample showed large nanoparticles of irregular shape and with a rough surface, indicating the successful exchange of protons by Sn ions, which was similar to our previously reported results (Cai et al., 2019). Moreover, **Figure 3c** shows a 100–200-nm size for the synthesized Cu-BTC nanoparticles, which are irregular octahedral crystals with low crystallinity and a

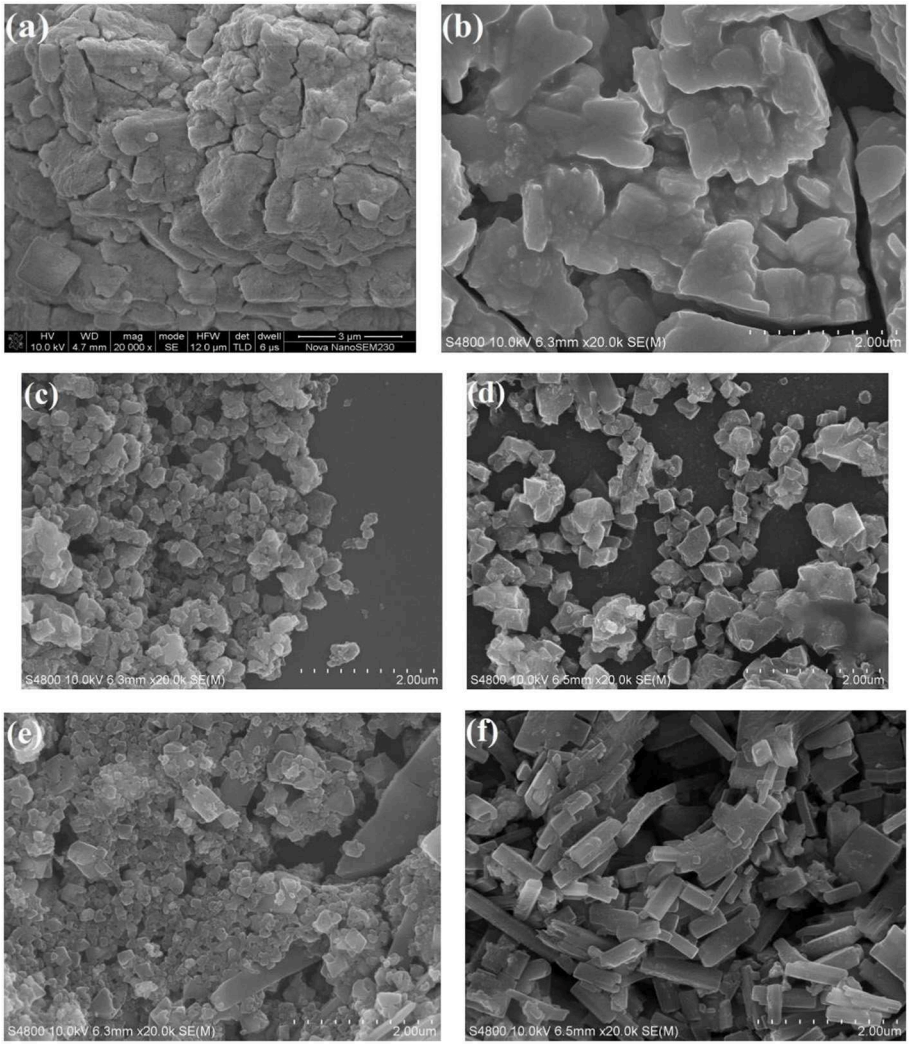

FIGURE 3 | SEM images of **(a)** pure HPW, **(b)** $Sn_{1.5}PW$, **(c)** Cu-BTC, **(d)** $Sn_{1.5}PW$/Cu-BTC-0.5, **(e)** $Sn_{1.5}PW$/Cu-BTC-1, and **(f)** $Sn_{1.5}PW$/Cu-BTC-1.5.

similar morphology as observed by Na et al. (2012). When $Sn_{1.5}PW$ was supported on Cu-BTC nanoparticles, the octahedral morphologies were markedly improved, suggesting that the addition of $Sn_{1.5}PW$ can be a modulator. Of note, the images (**Figures 3d–f**) showed a gradual increase in the $Sn_{1.5}PW$ coating on the surface of Cu-BTC nanoparticles, and, at 0.5 g $Sn_{1.5}PW$ loading, the surface morphology of $Sn_{1.5}PW$/Cu-BTC-1 was smooth, with no Sn1.5PW agglomeration. This observation might be due to the Cu-BTC matrix being completely coated. Meanwhile, compared to $Sn_{1.5}PW$/Cu-BTC-0.5 and $Sn_{1.5}PW$/Cu-BTC-1.5, the particle size of $Sn_{1.5}PW$/Cu-BTC-1 hybrids, which was in a range of 100–250 nm, was lower; thus, the $Sn_{1.5}PW$/Cu-BTC-1 hybrids possessed a high specific surface. Based on the above analyses, $Sn_{1.5}PW$/Cu-BTC-1 was selected for further characterization.

To visualize $Sn_{1.5}PW$ supported on Cu-BTC, TEM images of the $Sn_{1.5}PW$/Cu-BTC-1 were acquired; these are shown in **Figure 4**. From **Figure 4a**, it can be seen that the $Sn_{1.5}PW$/Cu-BTC-1 presented an octahedral shape, confirming that the framework of Cu-BTC was properly retained. As highlighted in **Figures 4b,c**, the edges became noticeably roughened, and this reveals that many small $Sn_{1.5}PW$ particles were relatively uniformly distributed on the edges, which is consistent with the XRD and SEM results.

The N_2 adsorption-desorption isotherms and BJH pore size distributions of Cu-BTC and $Sn_{1.5}PW$/Cu-BTC-1 samples are shown in **Figure 5**. All samples show a type I isotherm, which revealed their microporous nature. Of note, the pore size distribution (**Figure 5B**) proved that the pores had an average diameter of 2–10 nm and a narrow size distribution. Moreover, the surface area decreased from 578.2 to 29.7 m^2/g, and the average pore size increased from 2.38 to 7.11 nm for Cu-BTC and $Sn_{1.5}PW$/Cu-BTC-1, respectively. The decrease in the BET surface area may be attributed to the presence

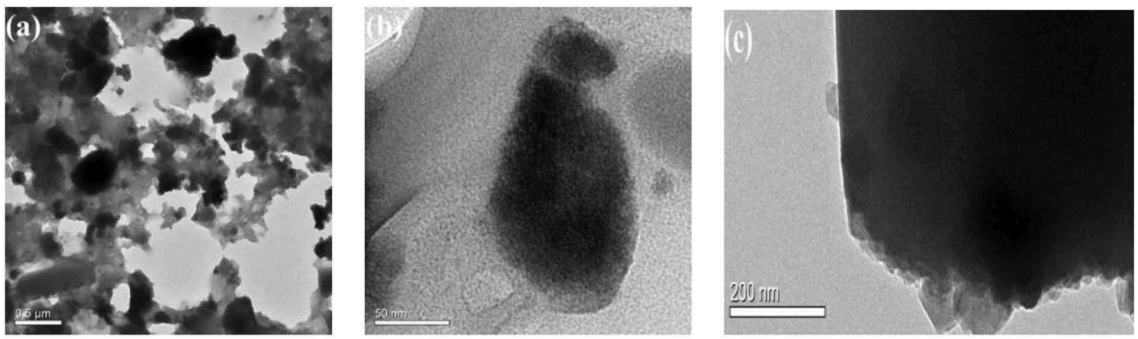

FIGURE 4 | (a–c) Typical TEM images of the $Sn_{1.5}PW$/Cu-BTC-1 hybrids.

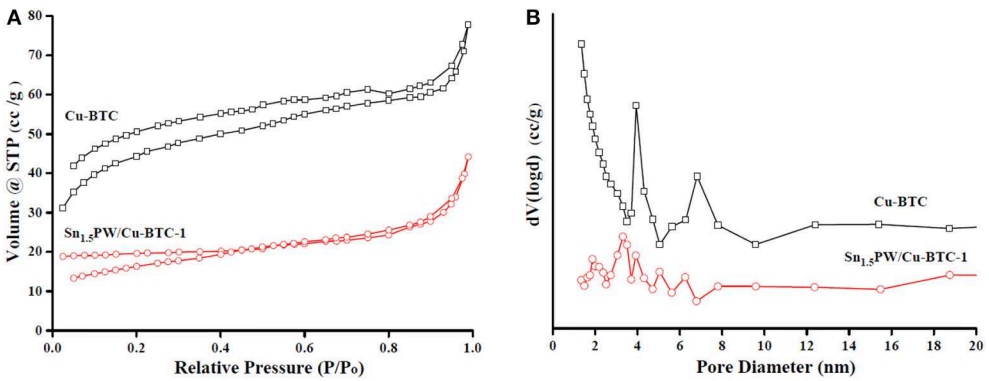

FIGURE 5 | (A) N_2 adsorption-desorption isotherm plots and **(B)** pore size distributions of Cu-BTC and $Sn_{1.5}PW$/Cu-BTC-1 samples.

of $Sn_{1.5}PW$ inside the Cu-BTC nanocages. The increase in the average pore size was probably due to a collapsed microporous structure, which was similar to previously reported results (Jeona et al., 2019). Meanwhile, the open cavities and relatively high specific surface area of $Sn_{1.5}PW$/Cu-BTC-1 nanocomposites were retained, which made for the free diffusion of the reactants or products, consistent with SEM results.

The thermal stabilities of the $Sn_{1.5}PW$, Cu-BTC, and $Sn_{1.5}PW$/Cu-BTC-1 samples were established with TG analysis (**Figure 6**). The $Sn_{1.5}PW$ sample showed no significant decomposition, and only 6% mass loss was observed up to 600°C. For the Cu-BTC and $Sn_{1.5}PW$/Cu-BTC-1 samples, the TG curve exhibited two stages of mass-loss, namely 40–250 and 250–400°C; these intervals can be associated with the release of physically adsorbed water on the surface of sample and bonded water from the crystal hydrates (Azmoon et al., 2019) and the decomposition of the Cu-BTC frameworks (Xie and Wan, 2018), respectively. Above 400°C, almost no obvious mass loss was observed in the TG curve. The results indicated that the prepared catalysts had better stability and could be employed as heterogeneous catalysts for the esterification reaction.

Figure 7 displays the NH_3-TPD profiles of $Sn_{1.5}PW$/Cu-BTC-1 nanocomposites. The minimum and maximum desorption temperatures of NH_3 are 225 and 319°C. The acidity present is attributed to the surface acidity of $Sn_{1.5}PW$. Based on these results, the nanocomposites possessed 24.6 mmol/g of total acidity. The results of NH_3-TPD also show that the catalyst

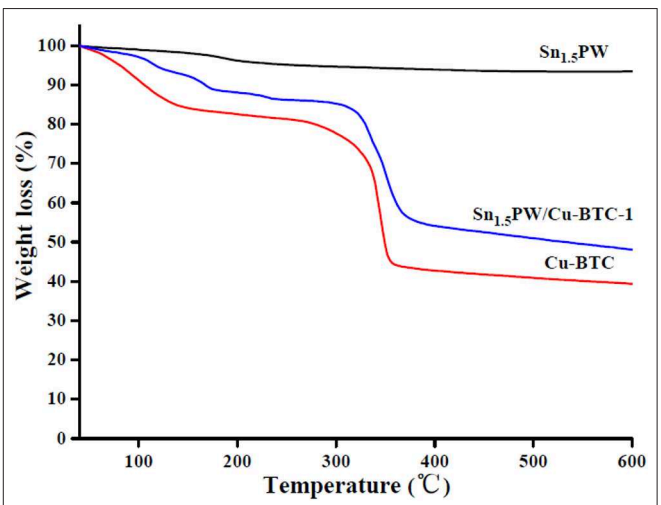

FIGURE 6 | TG curves of $Sn_{1.5}PW$, Cu-BTC, and $Sn_{1.5}PW$/Cu-BTC-1 samples.

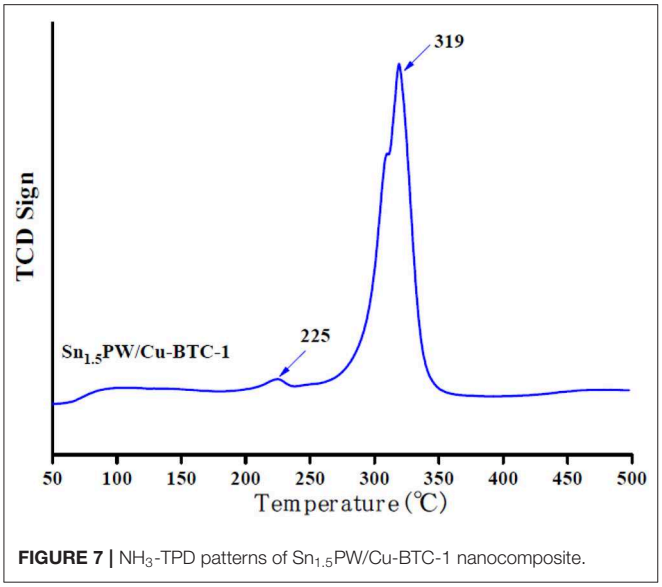

FIGURE 7 | NH_3-TPD patterns of $Sn_{1.5}PW/Cu\text{-}BTC\text{-}1$ nanocomposite.

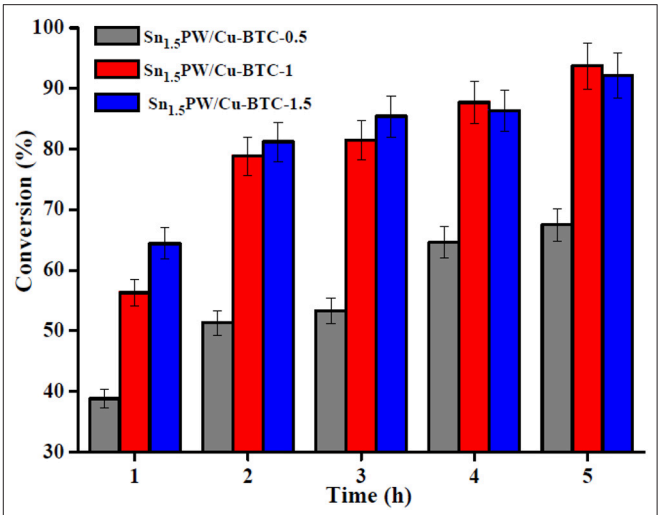

FIGURE 8 | Effects of various nanocatalysts for esterification of OA.

performance can be correlated with low and medium acidity strength. Therefore, the $Sn_{1.5}PW/Cu\text{-}BTC\text{-}1$ nanocomposites exhibit higher catalytic activity in the OA esterification.

Catalytic Performance of Different Catalysts

The influence of the molar ratio of $Sn_{1.5}PW/Cu\text{-}BTC$ on the esterification of OA was studied at 160°C by using 0.2 g catalyst and a 1:20 OA to methanol molar ratio within 4 h of reaction time. The results in **Figure 8** reveal that the OA conversion was enhanced with the increase of the $Sn_{1.5}PW/Cu\text{-}BTC$ ratio up to 1. The highest OA conversion was obtained by utilizing $Sn_{1.5}PW/Cu\text{-}BTC\text{-}1$ and $Sn_{1.5}PW/Cu\text{-}BTC\text{-}1.5$ at 5 h. Most probably, this increase in the catalytic activity can be attributed to its relatively large specific surface area and appropriate particle size. In order to save raw material and avoid $Sn_{1.5}PW$ agglomeration on the support surface, we used this $Sn_{1.5}PW/Cu\text{-}BTC\text{-}1$ as the catalyst for further research.

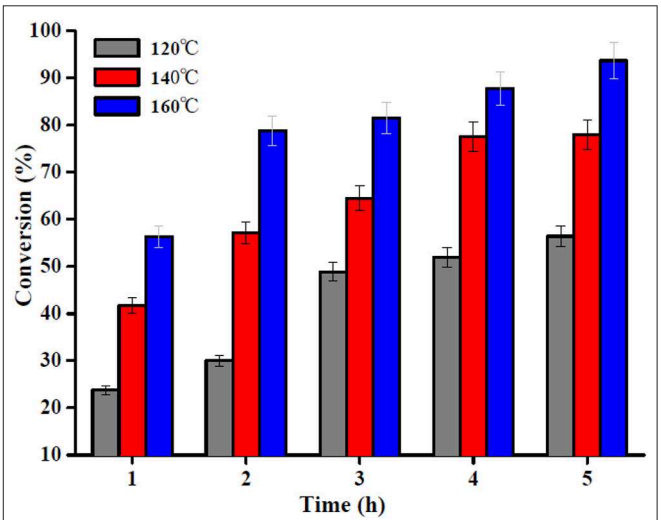

FIGURE 9 | Effect of reaction time and temperature. Reaction conditions: OA/methanol molar ratio 1:20, catalyst amount 0.2 g.

Effect of Esterification Conditions

Biodiesel was produced by esterification, which is a reversible reaction that converts the OA into methyl oleate (biodiesel) and water in the presence of a nanocatalyst such as the $Sn_{1.5}PW/Cu\text{-}BTC\text{-}1$. The reaction temperature is one of the key parameters of the esterification reaction. Thus, the effect of temperature in the range 120–160°C on the esterification reaction of OA with methanol with $Sn_{1.5}PW/Cu\text{-}BTC\text{-}1$ nanocatalyst was examined, and the results are presented in **Figure 9**. The results indicated that the OA conversion was improved with an increase in the temperature, which indicates that high temperature would improve the $Sn_{1.5}PW/Cu\text{-}BTC\text{-}1$ catalytic activity due to the endothermic nature of the esterification reaction. When the temperature rose to 160°C, the OA conversion increased to 87.7% at 4 h. Moreover, the OA conversion was increased as the reaction time was increased from 1 to 4 h, but no significant increase in OA conversion was observed beyond 4 h until 5 h. Thus, the selected temperature and time for further studies were 160°C and 4 h, respectively.

The OA to methanol molar ratio is one of the most important factors affecting the OA conversion and the cost of biodiesel production. Therefore, the effect of the OA to methanol molar ratio on OA esterification to biodiesel is shown in **Figure 10A**. Since esterification is a reversible reaction, high OA conversion could be achieved by using excess methanol in the reaction. It is evident that with the increase in the molar ratio of OA to methanol from 1:10 to 1:20, the OA conversion increased somewhat; however, no important change occurred as the molar ratio increased up to 1:30, and a large amount of methanol probably affected the OA conversion adversely, as the reactant was diluted and reduced the OA concentration (Nandiwale et al.,

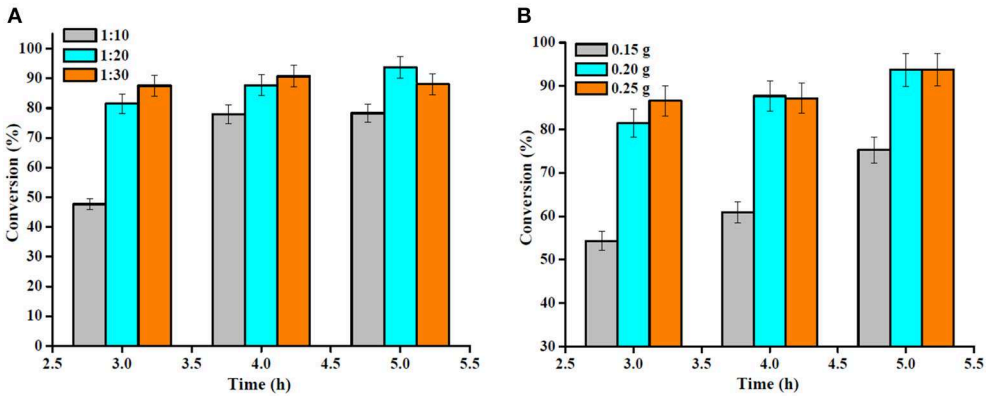

FIGURE 10 | (A) Effect of the molar ratio of OA to methanol (reaction conditions: temperature 160°C, catalyst amount 0.2 g) and **(B)** catalyst amount (reaction conditions: temperature 160°C, OA/methanol molar ratio 1:20).

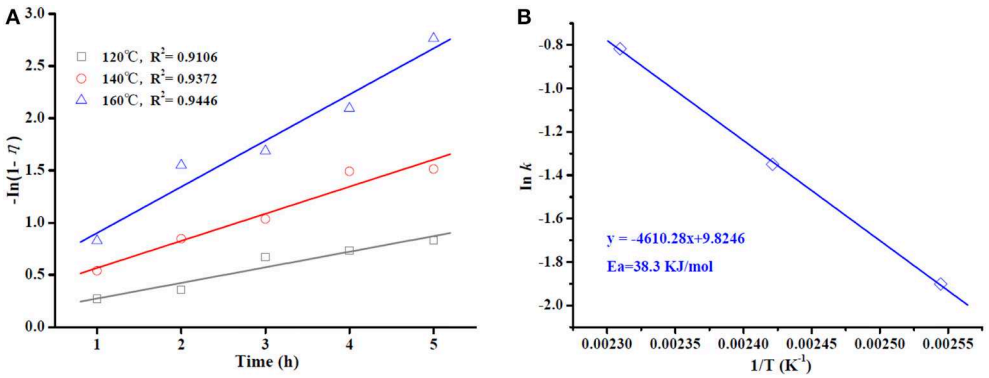

FIGURE 11 | Plot of -ln (1-η) vs. reaction time at different temperatures **(A)**. Arrhenius plot of ln *k* vs. 1/T **(B)**.

2013). Hence, the OA to methanol molar ratio was restricted to 1:20.

The study was further extended to the investigation of the effect of catalyst amount on the OA esterification reaction (**Figure 10B**). Under similar operating conditions, the OA conversion reached after 4 h of reaction was 60.9 and 87.7% using a $Sn_{1.5}$PW/Cu-BTC-1 nanocatalyst amount of 0.15 and 0.20 g, respectively. This is attributed to the acceleration of the reaction rate by there being a larger number of active sites in the reaction mixture. However, when a catalyst amount of 0.25 g was used, an OA conversion of 87.2% was reached, remaining practically constant in comparison with a catalyst amount of 0.20 g. Thus, it is suggested that 0.2 g of $Sn_{1.5}$PW/Cu-BTC-1 was the optimum amount, and this was used in the subsequent reactions.

Kinetic Studies of Biodiesel Production Using $Sn_{1.5}$PW/Cu-BTC-1 Nanocatalyst

Kinetic study for the OA esterification process was conducted under optimal conditions for $Sn_{1.5}$PW/Cu-BTC-1 at three different temperatures (120, 140, and 160°C). Because an excess

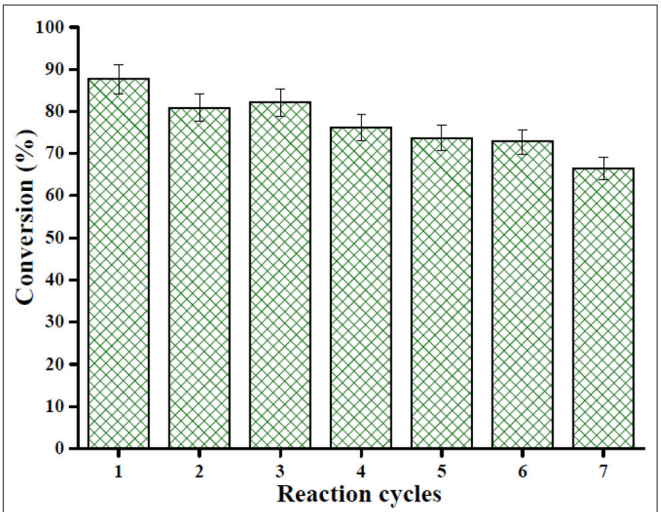

FIGURE 12 | Reusability of the nanocatalyst $Sn_{1.5}$PW/Cu-BTC-1 for seven cycles under optimum esterification conditions: temperature 160°C, catalyst amount 0.2 g, reaction time 4 h, and OA-methanol molar ratio 1:20.

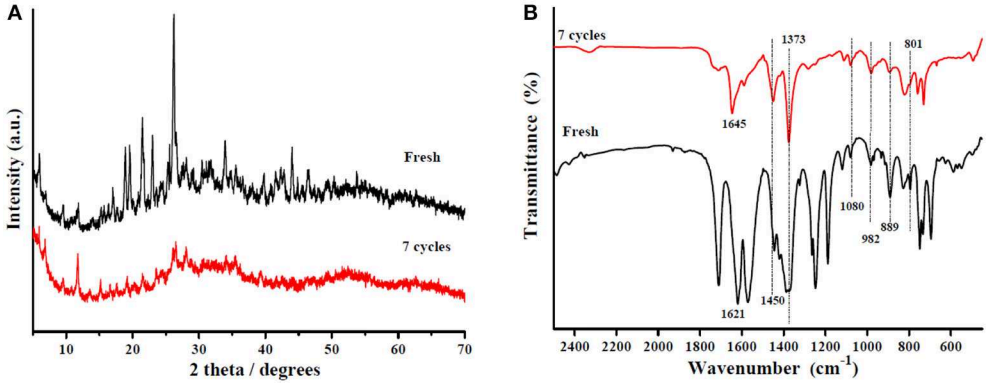

FIGURE 13 | (A) XRD patterns of the $Sn_{1.5}PW$/Cu-BTC-1 nanocatalyst and the nanocatalyst after seven cycles. **(B)** FT-IR spectra of the $Sn_{1.5}PW$/Cu-BTC-1 nanocatalyst and the nanocatalyst after seven cycles.

amount of methanol was used, the reverse reaction can be ignored, and the esterification reaction can also be assumed to follow the pseudo-first-order kinetic model (Kaur and Ali, 2015; Shalini and Chandra, 2018). Thus, the reaction rate constant is fitted in Equation (1), and the activation energy (E_a) required for the esterification process is calculated according to the Arrhenius, Equation (2).

$$k = -\mathrm{In}\frac{1-\eta}{t} \quad (1)$$

$$\mathrm{In}k = \mathrm{In}A - \frac{E_a}{RT} \quad (2)$$

where k is the reaction rate constant; η is the conversion of OA at time t; A is the Arrhenius constant or frequency factor; R is the universal gas constant; T is a reaction temperature.

A graph of ln (1-η) vs. time is given in **Figure 11A**. The plots display decent linearity with high regression coefficients (R^2 = 0.9106, 0.9372, and 0.9446 for 120, 140, and 160°C, respectively), indicating that the model is appropriate in terms of pseudo-first-order kinetics. The plot of ln k vs. 1/T in **Figure 11B** is found to be linear, with a high regression coefficient (R^2 = 0.9994). The value of E_a was determined to be 38.3 kJ/mol, which is much lower than the values determined in the works of Lieu et al. (2016) and Mazubert et al. (2014) for similar systems. More importantly, a value of $E_a > 15$ kJ/mol further supports that the OA esterification process in this work is controlled chemically (Patel and Brahmkhatri, 2013).

Reusability of Catalyst

Reusability is considered the most important characteristic of heterogeneous solid acid catalysts. In this work, the $Sn_{1.5}PW$/Cu-BTC-1 nanocatalyst was separated by centrifugation after the completion of the reaction, washed with anhydrous methanol, and then used directly after each cycle. Under the same optimum conditions, the esterification of OA was performed seven times, and **Figure 12** displays the results obtained. It was detected that the activity of the catalyst can still keep the conversion above 80% after three-time reuse. Nevertheless, it was found that, after seven times, the conversion was more than 60%. Furthermore, XRD and FT-IR tests were performed to determine the stability of the synthesized nanocatalyst; the results are presented in **Figures 13A,B**. According to **Figure 13A**, the XRD pattern of the recycled catalyst was almost consistent with that of the fresh one, and only the peak intensity decreased. As exhibited in **Figure 13B**, the featured peaks of the Keggin structure and the characteristic peaks of Cu-BTC were found in the FT-IR spectrum of the recycled catalyst, indicating that the $Sn_{1.5}PW$/Cu-BTC-1 nanocatalyst had a durable structure. Based on the above discussion, the catalytic activity loss might be due to the composites in the reaction mixture losing few $Sn_{1.5}PW$ active sites. Thus, in comparison with earlier reported solid acid catalysts, the synthesized $Sn_{1.5}PW$/Cu-BTC-1 nanocatalyst showed better stability in biodiesel synthesis.

CONCLUSION

In summary, an efficient solid acid nanocatalyst, $Sn_{1.5}PW$/Cu-BTC-1, was prepared through the immobilization of $Sn_{1.5}PW$ salts on Cu-BTC. The prepared nanocomposites were then implemented for the production of biodiesel from OA and methanol. A high conversion of 87.7% was obtained under the optimized conditions of 160°C for 4 h with a molar ratio of OA to methanol of 1:20, and the addition of 0.2 g of catalyst. In addition, this nanocomposite catalyst showed good stability, and even after seven cycles of reuse, a considerable OA conversion could still be achieved. Moreover, a pseudo-first-order kinetic model was found to represent the data more appropriately, with the E_a of the reaction being 38.3 kJ/mol. The remarkable point in this study was the use of a facile, simple, and cheap method for the synthesis of $Sn_{1.5}PW$/Cu-BTC nanocomposites in the large-scale production of biodiesel.

DATA AVAILABILITY STATEMENT

The raw data supporting the conclusions of this article will be made available by the authors, without undue reservation, to any qualified researcher.

AUTHOR CONTRIBUTIONS

QZ was in charge of designing the experiments and writing the manuscript. DLi and DLe performed experiments. XL, JW, YZ, and PM were in charge of revising the manuscript.

FUNDING

This work was financially supported by the Guizhou Science and Technology Foundation ([2020]1Y054), the Technical Talent Support Program of Guizhou Education Department (KY [2018]069), the Academician Workstation of Guizhou Science and Technology Plan (S&T Cooperation Platform Talents [2016]5602), the Guizhou Science and Technology Cooperation Project (LH[2017]7059), the Key Support Discipline in Agricultural Resources and Environment of Anshun University, and the Creative Research Groups Support Program of Guizhou Education Department (KY [2017]049).

SUPPLEMENTARY MATERIAL

The Supplementary Material for this article can be found online at: https://www.frontiersin.org/articles/10.3389/fchem.2020.00129/full#supplementary-material

REFERENCES

Al-Saadi, L. S., Eze, V. C., and Harvey, A. P. (2018). Experimental determination of optimal conditions for reactive coupling of biodiesel production with in situ glycerol carbonate formation in a triglyceride transesterification process. *Front. Chem.* 6:625. doi: 10.3389/fchem.2018.00625

Azmoon, A. H., Ahmadpour, A., Nayebzadeh, H., Saghatoleslami, N., and Heydari, A. (2019). Fabrication of nanosized SO_4^{2-}/Co-Al mixed oxide via solution combustion method used in esterification reaction: effect of urea-nitrate ratio on the properties and performance. *J. Nanostruct. Chem.* 9, 247–258. doi: 10.1007/s40097-019-00315-y

Bhanja, P., and Bhaumik, A. (2016). Porous nanomaterials as green catalyst for the conversion of biomass to bioenergy. *Fuel* 185, 432–441. doi: 10.1016/j.fuel.2016.08.004

Cai, J., Yang, T. T., Yue, C. Y., Pu, Q. L., Wang, R. Y., and Zhang, Q. Y. (2019). Preparation of silver-exchanged heteropolyacid catalyst and its application for biodiesel production. *Energ. Source. Part A* 1–11. doi: 10.1080/15567036.2019.1623945

da Conceiçao, L. R. V., Carneiro, L. M., Giordani, D. S., and de Castro, H. F. (2017). Synthesis of biodiesel from macaw palm oil using mesoporous solid catalyst comprising 12-molybdophosphoric acid and niobia. *Renew. Energ.* 113, 119–128. doi: 10.1016/j.renene.2017.05.080

Ekinci, E. K., and Oktar, N. (2019). Production of value-added chemicals from esterification of waste glycerol over MCM-41 supported catalysts. *Green Process. Synth.* 8, 128–134. doi: 10.1515/gps-2018-0034

Ghubayra, R., Nuttall, C., Hodgkiss, S., Craven, M., Kozhevnikova, E. F., and Kozhevnikov, I. V. (2019). Oxidative desulfurization of model diesel fuel catalyzed by carbon-supported heteropoly acids. *Appl. Catal. B Environ.* 253, 309–316. doi: 10.1016/j.apcatb.2019.04.063

Hu, P. F., Chen, C. C., Wang, Y. F., Pan, L., and Lu, C. H. (2019). Room-temperature self-assembled preparation of porous $ZnFe_2O_4$/MIL-100(Fe) nanocomposites and their visible- light derived photocatalytic properties. *Chem. Select* 4, 9703–9709. doi: 10.1002/slct.201902246

Jeona, Y., Chia, W. S., Hwang, J., Kim, D. H., Kim, J. H., and Shul, Y. G. (2019). Core-shell nanostructured heteropoly acid-functionalized metal-organic frameworks: bifunctional heterogeneous catalyst for efficient biodiesel production. *Appl. Catal. B Environ.* 242, 51–59. doi: 10.1016/j.apcatb.2018.09.071

Kang, Y. S., Lu, Y., Chen, K., Zhao, Y., Wang, P., and Sun, W. Y. (2019). Metal-organic frameworks with catalytic centers: from synthesis to catalytic application. *Coordin. Chem. Rev.* 378, 262–280. doi: 10.1016/j.ccr.2018.02.009

Kaur, N., and Ali, A. (2015). Preparation and application of Ce/ZrO_2-TiO_2/SO_4^{2-} as solid catalyst for the esterification of fatty acids. *Renew. Energ.* 81, 421–431. doi: 10.1016/j.renene.2015.03.051

Li, D. D., Xu, H. O., Jiao, L., and Jiang, H. L. (2019). Metal-organic frameworks for catalysis: State of the art, challenges, and opportunities. *EnergyChem* 1:100005. doi: 10.1016/j.enchem.2019.100005

Li, H., Liu, F. S., Ma, X. L., Wu, Z. J., Li, Y., Zhang, L. H., et al. (2019). Catalytic performance of strontium oxide supported by MIL-100(Fe) derivate as transesterification catalyst for biodiesel production. *Energ. Convers. Manage.* 180, 401–410. doi: 10.1016/j.enconman.2018.11.012

Li, H., Wang, C. H., Xu, Y. F., Yu, Z. Z., Saravanamurugan, S., Wu, Z. L., et al. (2020). Heterogeneous (de) chlorination-enabled control of reactivity in the liquid-phase synthesis of furanic biofuel from cellulosic feedstock. *Green Chem.* 22, 637–645 doi: 10.1039/C9GC04092G

Lieu, T., Yusup, S., and Moniruzzaman, M. (2016). Kinetic study on microwave-assisted esterification of free fatty acids derived from Ceiba pentandra seed oil. *Bioresour. Technol.* 211, 248–256. doi: 10.1016/j.biortech.2016.03.105

Long, J., Xu, Y., Zhao, W., Li, H., and Yang, S. (2019). Heterogeneous catalytic upgrading of biofuranic aldehydes to alcohols. *Front. Chem.* 7:529. doi: 10.3389/fchem.2019.00529

Mahmoud, H. R. (2019). Bismuth silicate ($Bi_4Si_3O_{12}$ and Bi_2SiO_5) prepared by ultrasonic-assisted hydrothermal method as novel catalysts for biodiesel production via oleic acid esterification with methanol. *Fuel* 256:115979. doi: 10.1016/j.fuel.2019.115979

Mazubert, A., Taylor, C., Aubin, J., and Poux, M. (2014). Key role of temperature monitoring in interpretation of microwave effect on transesterification and esterification reactions for biodiesel production. *Bioresour. Technol.* 161, 270–279. doi: 10.1016/j.biortech.2014.03.011

Na, L. Y., Hua, R. N., Ning, G. L., and Ou, X. X. (2012). Nano/micro HKUST-1 fabricated by coordination modulation method at room temperature. *Chem. Res. Chin. Univ.* 28, 555–558.

Nandiwale, K. Y., and Bokade, V. V. (2014). Process optimization by response surface methodology and kinetic modeling for synthesis of methyl oleate biodiesel over $H_3PW_{12}O_{40}$ anchored montmorillonite K10. *Ind. Eng. Chem. Res.* 53, 18690–18698. doi: 10.1021/ie500672v

Nandiwale, K. Y., Sonar, S. K., Niphadkar, P. S., Joshi, P. N., Deshpande, S. S., Patil, V. S., et al. (2013). Catalytic upgrading of renewable levulinic acid to ethyl levulinate biodiesel using dodecatungstophosphoric acid supported on desilicated H-ZSM-5 as catalyst. *Appl. Catal. A Gen.* 460–461, 90–98. doi: 10.1016/j.apcata.2013.04.024

Negm, N. A., Betiha, M. A., Alhumaimess, M. S., Hassan, H. M. A., and Rabie, A. M. (2019). Clean transesterification process for biodiesel production using heterogeneous polymer-heteropoly acid nanocatalyst. *J. Clean. Prod.* 238:117854. doi: 10.1016/j.jclepro.2019.117854

Nikseresht, A., Daniyali, A., Ali-Mohammadi, M., Afzalinia, A., and Mirzaie, A. (2017). Ultrasound-assisted biodiesel production by a novel composite of Fe (III)-based MOF and phosphotangestic acid as efficient and reusable catalyst. *Ultrason. Sonochem.* 37, 203–207. doi: 10.1016/j.ultsonch.2017.01.011

Parida, K. M., and Mallick, S. (2007). Silicotungstic acid supported zirconia: an effective catalyst for esterification reaction. *J. Mol. Catal. A Chem.* 275, 77–83. doi: 10.1016/j.molcata.2007.05.022

Pasha, N., Lingaiah, N., and Shiva, R. (2019). Zirconium exchanged phosphotungstic acid catalysts for esterification of levulinic acid to ethyl levulinate. *Catal. Lett.* 149, 2500–2507. doi: 10.1007/s10562-019-02862-z

Patel, A., and Brahmkhatri, V. (2013). Kinetic study of oleic acid esterification over 12-tungstophosphoric acid catalyst anchored to different mesoporous silica supports. *Fuel Process. Technol.* 113, 141–149. doi: 10.1016/j.fuproc.2013.03.022

Shalini, S., and Chandra, S. Y. (2018). Economically viable production of biodiesel using a novel heterogeneous catalyst: kinetic and thermodynamic investigations. *Energ. Convers. Manage.* 171, 969–983. doi: 10.1016/j.enconman.2018.06.059

Sun, Z., Duan, X. X., Zhao, J., Wang, X. H., and Jiang, Z. J. (2015). Homogeneous borotungstic acid and heterogeneous micellar borotungstic acid catalysts for biodiesel production by esterification of free fatty acid. *Biomass Bioenerg.* 76, 31–42. doi: 10.1016/j.biombioe.2015.03.002

Talebian-Kiakalaieh, A., Amin, N. A. S., Zarei, A., and Noshadi, I. (2013). Transesterification of waste cooking oil by heteropoly acid (hpa) catalyst: optimization and kinetic model. *Appl. Energ.* 102, 283–292. doi: 10.1016/j.apenergy.2012.07.018

Xie, W. L., and Wan, F. (2018). Basic ionic liquid functionalized magnetically responsive Fe_3O_4@HKUST-1 composites used for biodiesel production. *Fuel* 220, 248–256. doi: 10.1016/j.fuel.2018.02.014

Xie, W. L., and Wan, F. (2019a). Biodiesel production from acidic oils using polyoxometalate-based sulfonated ionic liquids functionalized metal-organic frameworks. *Catal. Lett.* 149, 2916–2929. doi: 10.1007/s10562-019-02800-z

Xie, W. L., and Wan, F. (2019b). Immobilization of polyoxometalate-based sulfonated ionic liquids on UiO-66-2COOH metal-organic frameworks for biodiesel production via one-pot transesterification-esterification of acidic vegetable oils. *Chem. Eng. J.* 365, 40–50. doi: 10.1016/j.cej.2019.02.016

Xu, Y. F., Long, J. X., Zhao, W. F., Li, H., and Yang, S. (2019). Efficient transfer hydrogenation of nitro compounds to amines enabled by mesoporous N-stabilized Co-Zn/C. *Front. Chem.* 7:590. doi: 10.3389/fchem.2019.00590

Yang, X. L., Qiao, L., and Dai, W. (2015). One-pot synthesis of a hierarchical microporous-mesoporous phosphotungstic acid-HKUST-1 catalyst and its application in the selective oxidation of cyclopentene to glutaraldehyde. *Chin. J. Catal.* 36, 1875–1885. doi: 10.1016/S1872-2067(15)60972-X

Zhang, D. Y., Duan, M. H., Yao, X. H., Fu, Y. J., and Zu, Y. G. (2016). Preparation of a novel cellulose-based immobilized heteropoly acid system and its application on the biodiesel production. *Fuel* 172, 293–300. doi: 10.1016/j.fuel.2015.12.020

Zhang, Q. Y., Ling, D., Lei, D. D., Deng, T. L., Zhang, Y. T., and Ma, P. H. (2020). Synthesis and catalytic properties of nickel salts of keggin-type heteropolyacids embedded metal-organic framework hybrid nanocatalyst. *Green Process. Synth.* 9, 131–138. doi: 10.1515/gps-2020-0014

Zhang, Q. Y., Yang, T. T., Liu, X. F., Yue, C. Y., Ao, L. F., Deng, T. L., et al. (2019b). Heteropoly acid-encapsulated metal-organic framework as a stable and highly efficient nanocatalyst for esterification reaction. *RSC Adv.* 9, 16357–16365. doi: 10.1039/C9RA03209F

Zhang, Q. Y., Yue, C. Y., Pu, Q. L., Yang, T. T., Wu, Z. F., and Zhang, Y. T. (2019a). Facile synthesis of ferric-modified phosphomolybdic acid composite catalysts for biodiesel production with response surface optimization. *ACS Omega* 4, 9041–9048. doi: 10.1021/acsomega.9b01037

Conflict of Interest: The authors declare that the research was conducted in the absence of any commercial or financial relationships that could be construed as a potential conflict of interest.